Japanese Journal of Applied Physics

The Japan Society of Applied Physics

REGULAR PAPER

Etching characteristics and mechanisms of Mo thin films in Cl_2/Ar and CF_4/Ar inductively coupled plasmas

To cite this article: Nomin Lim *et al* 2014 *Jpn. J. Appl. Phys.* **53** 116201

View the article online for updates and enhancements.

Related content

- Etching characteristics of Pb(Zr,Ti)O3, Pt, SiO2 and Si3N4 in an inductively coupled HBr/Ar plasma
Alexander Efremov, Nam Ki Min, Jaehwa Jeong et al.

- Etching characteristics of SiC, SiO_2, and Si in CF_4/CH_2F_2/N_2/Ar inductively coupled plasma: Effect of CF_4/CH_2F_2 mixing ratio
Jongchan Lee, Alexander Efremov, Kwangsoo Kim et al.

- Etching Characteristics of In_2O_3 and SnO_2 Thin Films in an Inductively Coupled HBr/Ar Plasma: Effects of Gas Mixing Ratio and Bias Power
Kwang-Ho Kwon, Alexander Efremov, Moonkeun Kim et al.

This content was downloaded from IP address 115.145.196.110 on 12/12/2017 at 01:50

Japanese Journal of Applied Physics **53**, 116201 (2014) **REGULAR PAPER**
http://dx.doi.org/10.7567/JJAP.53.116201

Etching characteristics and mechanisms of Mo thin films in Cl_2/Ar and CF_4/Ar inductively coupled plasmas

Nomin Lim[1], Alexander Efremov[2], Geun Young Yeom[3], Bok-Gil Choi[4], and Kwang-Ho Kwon[1*]

[1]*Department of Control and Instrumentation Engineering, Korea University, Sejong 339-700, Republic of Korea*
[2]*Department of Electronic Devices and Materials Technology, State University of Chemistry and Technology, Ivanovo 153000, Russia*
[3]*Department of Advanced Materials Science and Engineering, Sungkyunkwan University, Suwon, Gyeonggi 440-746, Republic of Korea*
[4]*Department of Electrical Engineering, Kongju National University, Gongju, Chungnam 314-701, Republic of Korea*
E-mail: kwonkh@korea.ac.kr

Received April 28, 2014; accepted June 23, 2014; published online October 2, 2014

The etching characteristics and mechanism of Mo thin films in Cl_2/Ar and CF_4/Ar inductively coupled plasmas under the same operating conditions (pressure, 6 mTorr; input power, 700 W; bias power, 200 W) were investigated. For both gas mixtures, an increase in the Ar fraction or gas pressure at a fixed gas mixing ratio was found to cause a non-monotonic change in the Mo etching rates. The X-ray photoelectron spectroscopy (XPS) diagnostics indicated contamination of the etched surfaces by reaction products. The Cl_2/Ar and CF_4/Ar plasma parameters were also investigated using a combination of a zero-dimensional plasma model and plasma diagnostics using Langmuir probes. An analysis of the etching kinetics with the model-predicted fluxes of the plasma active species suggests that: 1) the Mo etching process occurs in the transitional regime of the ion-assisted chemical reaction, and 2) the non-monotonic Mo etching rate is probably associated with opposing changes in the fluxes of the reactive neutral species and ion energy. © 2014 The Japan Society of Applied Physics

1. Introduction

During the last decade, refractory metals such as Mo, W, and Ta have been of great interest to electronic device developers. Because of their low resistivity and good thermal properties, these metals are the most likely substitutes for poly-Si for use as gate electrodes in field-effect transistors.[1,2] In particular, Mo was found to combine easily with Al_2O_3,[3] which is one of the most promising gate dielectrics owing to its high dielectric constant of ~8 (compared with ~3.9 for SiO_2), low leakage current, high breakdown strength, and good thermodynamic stability in contact with Si.[4] Moreover, Mo is a promising material for bulk microelectromechanical systems applications owing to its high melting point, radiation resistance, high strength, and conductivity.[5] Therefore, the development and optimization of the dry etching process for both Mo thin films and bulk material is important for modern plasma etching technology. This task cannot be completed without knowledge of the Mo etching mechanism and an understanding of the relationships between the input process parameters and output characteristics.

Several studies have investigated the Mo etching process with both chlorine-[6,7] and fluorine-based[2,8] plasma chemistries. One of the most important conclusions reported in these works is that, in both gas systems, the "dry" etching of Mo is driven by the chemical etching pathway. This conclusion is supported by the strong dependence of the Mo etching rate on the surface temperature[6] and its proportionality with the Cl atom density.[7] It has also been reported that the Mo etching process in CF_4- and SF_6-based plasmas can be noticeably accelerated by the addition of O_2.[8] A similar phenomenon has been repeatedly reported for both poly- and mono-Si and is connected with an increase in the formation rate and volume density of F atoms.[6,9] However, the following points must be considered when analyzing existing works: 1) because most of these papers were published in the 1980s and 1990s, several of these results were obtained for plate-parallel reactive-ion etching (RIE) reactors; 2) the conclusions regarding the Mo etching mechanism were based on the dependence of the etching rates on the main operating parameters, although the relationships between the etching rates, plasma parameters, and composition were not explored; and 3) among the investigated effects of the input process parameters on the Mo etching rate, the gas mixing ratio received the least attention. Moreover, if a mixture of a chemically active gas and a noble gas is used for etching, the gas mixing ratio provides more information on the etching mechanism because it directly reflects the transition between the chemical and physical etching pathways.

In this work, we conducted a model-based comparative study of the Mo etching characteristics and mechanisms in Cl_2/Ar and CF_4/Ar plasmas by considering the changes in the plasma parameters and densities of the plasma active species under the same operating conditions. We would like to emphasize that although several works have been published on both the diagnostics and modeling of Cl_2/Ar and CF_4/Ar plasmas, it is not possible to directly compare these systems to analyze the etching mechanism. This is because of the different experimental conditions, modeling approaches, reactor types, and geometries used by various authors.

2. Experimental and modeling details

2.1 Film preparation

The Mo thin film was deposited on a Si(111) substrate. The films were produced by radio frequency magnetron sputtering using a Mo target. The sputtering process was conducted in Ar with a gas pressure of 2.25 mTorr and input power of 300 W. The substrate was maintained at room temperature. A deposition time of 15 min yielded a 150-nm-thick Mo film.

2.2 Plasma etching and diagnostics techniques

Both etching and plasma diagnostics experiments were performed in the planar inductively coupled plasma (ICP) reactor used in our previous works.[10,11] The reactor consisted of a cylindrical ($r = 16$ cm) chamber made from anodized aluminum and a 5-turn copper coil located above a 10-mm-thick horizontal quartz window. The coil was connected to a 13.56 MHz power supply. The distance l between the window and the bottom electrode, which was used as a substrate holder, was 12.8 cm. The bottom electrode was connected to

 © 2014 The Japan Society of Applied Physics

a 12.56 MHz power supply to maintain a negative dc bias voltage U_{dc}. The temperature of the bottom electrode was stabilized at 17 °C using a water-flow cooling system. The experiments were performed at a fixed input power ($W_{inp} = 700$ W) and bias power ($W_{dc} = 200$ W). The effect of the gas mixing ratio was investigated at a pressure p of 6 mTorr. The initial compositions of the Cl_2/Ar and CF_4/Ar gas mixtures were set within the range of 0–100% Ar by adjusting the partial flow rates of the corresponding pure gases within a constant total flow rate of $q = 50$ sccm. The effect of the gas pressure p in the range of 4–10 mTorr was investigated for two basic gas mixtures, halogen-rich plasmas (80% Cl_2 or CF_4 + 20% Ar) and Ar-rich plasmas (20% Cl_2 or CF_4 + 80% Ar).

The etched samples were approximately $2 \times 2\,\mathrm{cm}^2$ in size and were placed at the center of the bottom electrode. The Mo etched depths were measured using a surface profiler (Tencor Alpha-step 500). For this purpose, we developed line striping using photoresist (PR; AZ1512, positive) with a line width/spacing ratio of 2 µm/2 µm. The initial thickness of the PR layer was about 1.5 µm. The compositional changes in the etched Mo surfaces were investigated using X-ray photoelectron spectroscopy (XPS; ESCALAB 220-IXL) with an Al Kα source (1486.6 eV).

Plasma diagnostics was performed with a double Langmuir probe (LP; Plasmart DLP2000). The probes were installed through the viewport on the sidewall of the reactor chamber 5.7 cm above the bottom electrode and centered in the radial direction. The current–voltage (I–V) curves were analyzed to obtain the electron temperature T_e, ion current density J_+, floating potential U_f, and total positive ion density n_+ using the software supplied by the equipment manufacturer. The calculations were based on the Johnson–Malter double probe theory[12] with the Allen–Boyd–Reynolds approximation, $J_+ \cong 0.61 e n_+ v$, for the ion saturation current density.[9]

2.3 Plasma model

To obtain additional data on the plasma parameters, densities, and fluxes of active species, we applied a simplified global (zero-dimensional) model. The model was applied with volume-averaged plasma parameters and used a Maxwellian approximation for the electron energy distribution function (EEDF).[13,14] The applicability of the Maxwellian EEDFs to Ar, Cl_2, and CF_4 ICPs at low pressures has been demonstrated.[13,15,16] The experimental data on T_e and n_+ were used as the input model parameters. The calculations were based on the simultaneous solution of:

1) The steady-state ($dn/dt = 0$) equations of the chemical kinetics for neutral and charged species. These equations were written in a general form, $R_F - R_V = (k_S + 1/\tau_R)n$, where R_F and R_V are the volume-averaged formation and decay rates, respectively, in bulk plasma for a given type of species; n is the density; k_S is the first-order heterogeneous decay rate coefficient; and $\tau_R = \pi r^2 lp/q$ is the residence time. For neutral atomic species and radicals, we assumed $k_S \approx 2r/\gamma v_T$, where γ is the recombination probability, and $v_T = (8k_B T/\pi m)^{1/2}$. For simplicity, we used a constant temperature for the neutral particles, $T = 700$ K.[11,16] For positive ions, we used $k_S \approx v/d_c$, where $d_c = 0.5rl/(rh_l + lh_r)$. The ion Bohm velocities v as well as the parameters h_l and h_r determined by the ion mean free path λ_i are given by the low-pressure $[\lambda_i \leq (T_i/T_e)(r,l)]$ diffusion theory.[17] For negative ions, we applied $k_S = 0$.[17]
2) The quasi-neutrality conditions for both the volume densities ($n_e + n_- = n_+$) and fluxes ($\Gamma_e = \Gamma_+$) of the charged species.

The output model parameters were the rate coefficients for electron-impact processes, the densities of the rest charged species (electrons, negative ions), the densities of neutral ground-state species (Cl_2, Cl, CF_x, F), and their fluxes on the etched surface. For more details on the modeling algorithm, the list of processes considered in the models, and the remaining input data set, see our earlier works.[11,16]

3. Results and discussion

3.1 Etching rate and surface conditions

Figure 1(a) shows that an increase in the Ar mixing ratio causes the Mo etching rate in both gas mixtures to vary non-monotonically. In the Cl_2/Ar gas mixture, the maximum Mo etching rate of 165 nm/min corresponds to 60% Ar. This value is about twice that for a pure Cl_2 plasma (84 nm/min) and nearly 5 times higher than the sputtering rate in pure Ar plasma (32 nm/min). In the CF_4/Ar gas mixture, the maximum etching rate (305 nm/min) is achieved for 20% Ar. We obtained a weaker increase in the etching rate compared with that of pure CF_4 gas (by 1.4 times only), whereas the gap between the maximum etching rate and the sputtering rate in pure Ar plasma is much higher. Varying the gas pressure also causes the Mo etching rates to change non-monotonically [Fig. 1(b)]. In halogen-rich (20% Ar) plasmas, the dependences for Cl_2- and CF_4-based gas mixtures are quite similar. They are characterized by weak maxima at $p = 8$ mTorr and a general increase in the etching rate toward higher pressures. The same occurs for a Cl_2-based gas chemistry in Ar-rich (80% Ar) plasma. At the same time, the CF_4-based gas chemistry with 80% Ar exhibits a maximum etching rate of about 5–6 mTorr and shows a general decrease in etching rate toward higher pressures.

On the basis of the above data, some preliminary conclusions about the Mo etching mechanism can be drawn. First, the similar non-monotonic behavior of the Mo etching rates in Cl_2/Ar and CF_4/Ar plasmas probably indicates a similar limiting stage of the etching process and type of active species responsible for the volatilization of the surface atoms in both cases. Second, because the etching rate in both Cl_2 and CF_4 gases is significantly higher than that in Ar plasma, the chemistry involved in the etching pathway seems to be more effective than physical sputtering. The dominant etching pathway (and hence, the behavior of the etching rate versus the main operating parameters) in chemically active plasmas is known to depend strongly on the volatility of the reaction products.[17–19] To compare the volatilities of different solid compounds, it is sufficient to compare their melting points T_{mp} or, even better, their boiling points T_{bp}. The T_{bp} values for $MoCl_5$ and MoF_5 are 268 and 216 °C, respectively. Thus, both Mo chlorides and Mo fluorides are moderate- or low-volatility compounds. The XPS data in Fig. 2 show that for both the investigated gas chemistries, the given process conditions do not result in an etched surface completely free of reaction products. This implies that the Mo etching process in Cl_2/Ar or CF_4/Ar plasmas is an ion-assisted chemical

© 2014 The Japan Society of Applied Physics

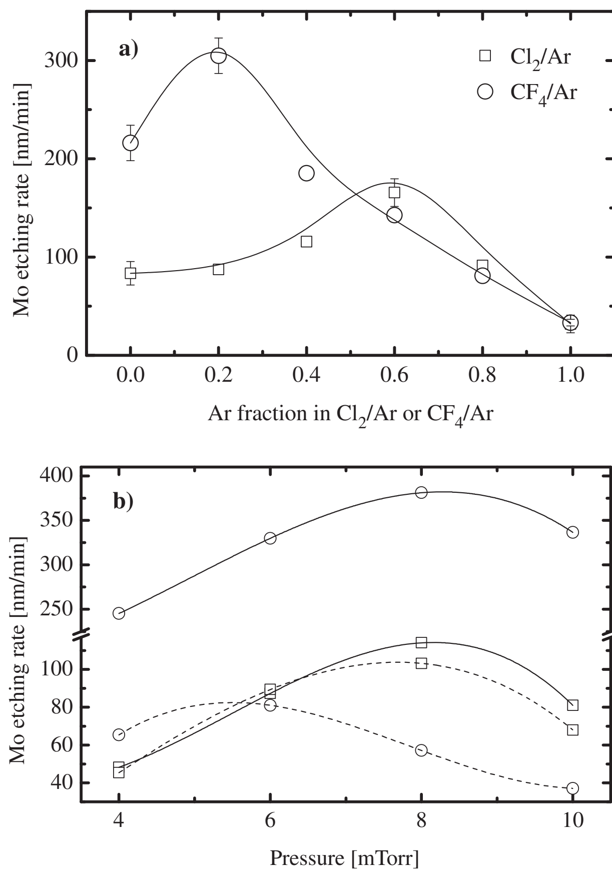

Fig. 1. Measured Mo etching rate as a function of (a) Ar fraction ($p = 6$ mTorr) and (b) gas pressure. In (b) solid lines correspond to halogen-rich plasmas (80% Cl_2 or CF_4 + 20% Ar), and dashed lines represent Ar-rich plasmas (20% Cl_2 or CF_4 + 80% Ar). The other process conditions are: $W = 700$ W and $W_{dc} = 200$ W. The lines are to guide the eye only.

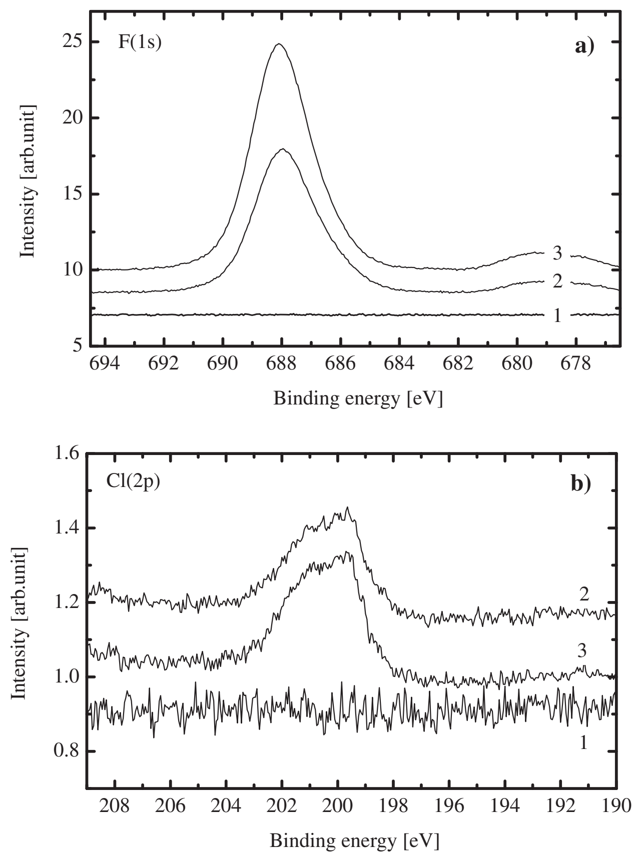

Fig. 2. (a) F 1s and (b) Cl 2p XPS narrow-scan spectra for samples etched using various gas mixing ratios for (1) as-deposited Mo film; (2) film etched in halogen-rich plasmas (20% Ar) at $p = 6$ mTorr, $W = 700$ W, and $W_{dc} = 200$ W; (3) film etched in Ar-rich plasmas (80% Ar) at $p = 6$ mTorr, $W = 700$ W, and $W_{dc} = 200$ W.

reaction that can occur in both reaction-rate-limited and ion-flux-limited etching regimes, depending on the balance between the formation and desorption rates for the reaction products.

Although all these suggestions look quite reasonable, at least two principal questions need to be answered for a complete understanding of the Mo etching mechanisms. The first is why the Mo etching rates change non-monotonically with respect to changes in the Ar mixing ratio and gas pressure. The second is why the etching rates at low Ar mixing ratios in the CF_4-based plasma are significantly higher. To address these questions, it is necessary to compare Cl_2/Ar or CF_4/Ar plasmas as the sources of active species and to analyze the correlations between the Mo etching rates, plasma parameters, and fluxes of plasma active species.

3.2 Comparative characterization of Cl_2/Ar and CF_4/Ar plasmas

Our earlier works presented detailed studies of the plasma chemistries in Cl_2/Ar and CF_4/Ar plasmas under a narrow range of experimental conditions and for ICP reactors of similar geometries.[11,16] Below, we will briefly summarize the most important issues in a comparative scale for a single set of process conditions.

Figures 3 and 4 show the results of plasma diagnostics by LPs. The increase in T_e with increasing Ar fraction [2.7–3.6 eV for Cl_2/Ar and 3.3–3.6 eV for CF_4/Ar at 0–100% Ar, Fig. 3(a)] results from the decreasing electron energy loss for electronic excitation and ionization.[15] This is because the corresponding processes for Ar atoms are characterized by higher energy thresholds and lower cross sections compared with those for Cl_2 and CF_4.[11,16] Therefore, because in the last case the gap between the threshold energies is lower, the change in T_e is smaller. A decrease in T_e with increasing gas pressure for both halogen- and Ar-rich plasmas [Fig. 3(b)] is associated with increasing electron energy loss due to an increase in the electron-neutral collision frequency.

Figure 4(a) shows that an increase in the Ar fraction in both Cl_2/Ar and CF_4/Ar plasmas results in quite similar changes in total positive ion density. Here, an increase in n_+ is associated with an increase in the total ionization frequency ($\nu_{iz} \approx k_1 n_{Cl_2} + k_3 n_{Ar}$ for Cl_2/Ar plasma and $\nu_{iz} \approx k_2 n_{CF_4} + k_3 n_{Ar}$ for CF_4/Ar plasma, where R1: $Cl_2 + e \rightarrow Cl_2^+ + 2e$, R2: $CF_4 + e \rightarrow CF_3^+ + F + 2e$, and R3: $Ar + e \rightarrow Ar^+ + 2e$) and with the change in the total balance of charged particles, which determines the plasma quasi-neutrality. The first effect occurs because the ionization rate coefficients k_1–k_3 follow the behavior of T_e, and the second is caused by the decreasing plasma electronegativity. In reality, in both gas systems the density of negative ions follows the decreasing dissociative attachment rate for Cl_2 or CF_4 molecules ($n_{Cl^-} = 4.7 \times 10^{10}$–$6.7 \times 10^9\ cm^{-3}$ in Cl_2/Ar plasma and

 © 2014 The Japan Society of Applied Physics

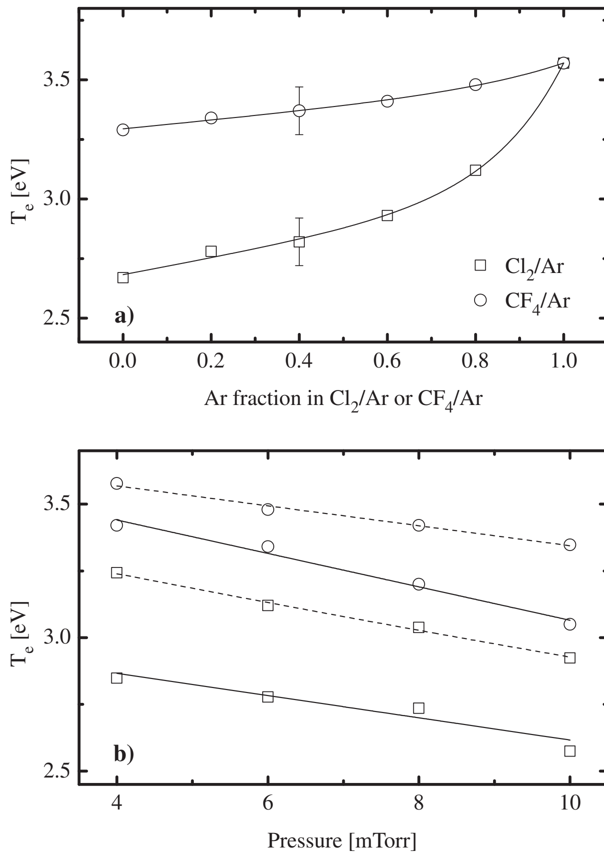

Fig. 3. Measured electron temperature as a function of (a) Ar fraction and (b) gas pressure. In (b), solid lines correspond to halogen-rich plasmas (20% Ar), and dashed lines represent Ar-rich plasmas (80% Ar). The other process conditions are the same as in Fig. 1.

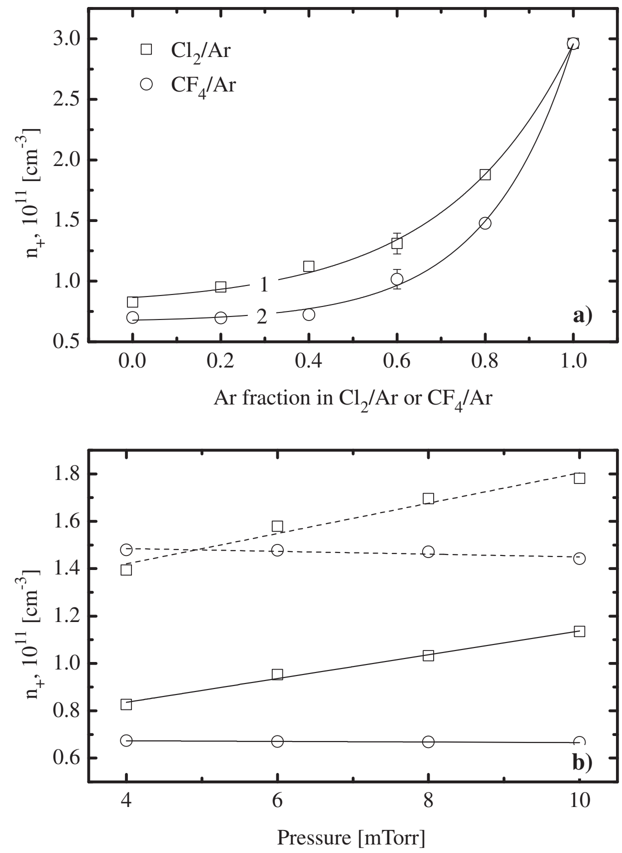

Fig. 4. Measured total positive ion density as a function of (a) Ar fraction and (b) gas pressure. In (b), solid lines correspond to halogen-rich plasmas (20% Ar), and dashed lines represent Ar-rich plasmas (80% Ar). The other process conditions are the same as in Fig. 1.

$n_{F^-} = 1.3 \times 10^{10}$–$2.7 \times 10^9\,cm^{-3}$ in CF_4/Ar plasma for 0–80% Ar), which corresponds to $n_{Cl^-}/n_e = 1.3$–0.05 and $n_{F^-}/n_e = 0.3$–0.02 [Fig. 5(a)]. These values are in good agreement with the published data for low-pressure electronegative plasmas, including Cl_2/Ar and CF_4/Ar ICPs.[11,16] An increase in the gas pressure results in increasing n_+ for Cl_2-based plasmas and in approximately constant n_+ for CF_4-based plasmas [Fig. 4(b)]. This difference is associated mainly with the different relative changes in k_1 and k_2, which are reflected in the behavior of ν_{iz}. Because the threshold energy for R2 is much higher than that for R1 (15.9 and 11.5 eV, respectively), the decrease in k_2 is more significant than that in k_1 for a similar decrease in T_e.

The model-predicted n_e as a function of the Ar fraction generally follows the behavior of n_+ [Fig. 5(a)]. A similar situation appears in the effect of the gas pressure in Ar-rich plasmas, where the relative density of negative ions in both gas chemistries does not exceed 0.1 [Fig. 5(c)]. In the halogen-rich plasmas, the density of negative ions at higher pressures becomes comparable to the electron density [$n_{Cl^-}/n_e = 0.5$–1.1 and $n_{F^-}/n_e = 0.1$–0.4 for $p = 4$–10 mTorr, Fig. 5(b)]. The quasi-neutrality condition requires a constant n_e (despite increasing n_+) for the Cl_2/Ar plasma and a decreasing n_e (despite constant n_+) for the CF_4/Ar plasma.

The neutral species of primary interest are Cl and F atoms. References 7 and 8 indicate that these species provide the chemical etching pathway for Mo in chlorine- and fluorine-based plasma chemistries, respectively. The addition of Ar to both Cl_2 and CF_4 was found to influence their dissociation kinetics though similar changes in T_e and n_e. In particular, in the Cl_2/Ar plasma, the effective dissociation rate coefficient $k_{dis} = 2k_5 + k_6 = 1.8 \times 10^{-8}$–$2.7 \times 10^{-8}\,cm^3/s$ for 0–100% Ar, where R5: $Cl_2 + e \rightarrow Cl + Cl + e$ and R6: $Cl_2 + e \rightarrow Cl + Cl^-$. Together with increasing n_e, this results in a noticeable increase in the dissociation frequency ($\nu_{dis} = k_{dis} n_e = 6.6 \times 10^2$–$7.8 \times 10^3\,s^{-1}$ for 0–100% Ar) and dissociation degree ($n_{Cl}/n_{Cl_2} = 3.2$–14.7 for 0–80% Ar), as well as in a slower than linear decrease in n_{Cl} [Fig. 6(a)]. An increase in the gas pressure results in an approximately constant ν_{dis} (1.1×10^3–$9.8 \times 10^2\,s^{-1}$ for a 20% Ar gas mixture and 3.2×10^3–$3.4 \times 10^3\,s^{-1}$ for an 80% Ar gas mixture at $p = 4$–10 mTorr) because of the opposite changes in T_e and n_e. As a result, in both Cl_2- and Ar-rich Cl_2/Ar plasmas, the total dissociation rate and Cl atom density follow the linearly increasing density of Cl_2 molecules in the feed gas.

In the CF_4/Ar plasma, the main source of F atoms is CF_4 molecules.[16] In this system, $k_{dis} = k_2 + k_7 = 2.1 \times 10^{-10}$–$3.3 \times 10^{-10}\,cm^3/s$ for 0–100% Ar (where R7: $CF_4 + e \rightarrow CF_3 + F + e$), $\nu_{dis} = 11.9$–$98.7\,s^{-1}$ for 0–100% Ar, and $n_F/n_{CF_4} = 0.5$–0.8 for 0–80% Ar. The smaller effect of the Ar fraction on the CF_4 dissociation kinetics compared with that in the Cl_2/Ar gas mixture is due to the smaller change in n_e. Here, the decreasing density of CF_4 molecules in the feed gas compensates for the weaker growth of ν_{dis}, and the density of F atoms falls linearly with increasing Ar mixing ratio [Fig. 6(b)]. An increase in the gas pressure results in

© 2014 The Japan Society of Applied Physics

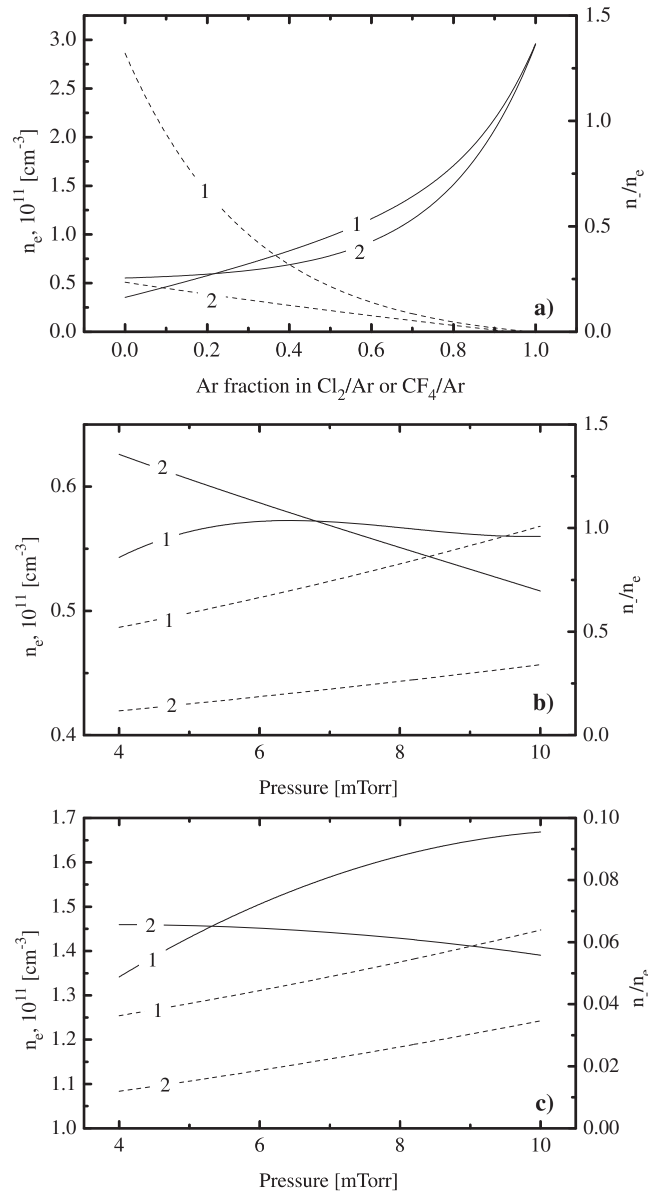

Fig. 5. Model-predicted electron density (solid lines) and relative density of negative ions (dashed lines) as functions of (a) Ar fraction and (b, c) gas pressure in (1) Cl_2/Ar and (2) CF_4/Ar plasmas. (b) Corresponds to halogen-rich plasmas (20% Ar), and (c) represents Ar-rich plasmas (80% Ar). The other process conditions are the same as in Fig. 1.

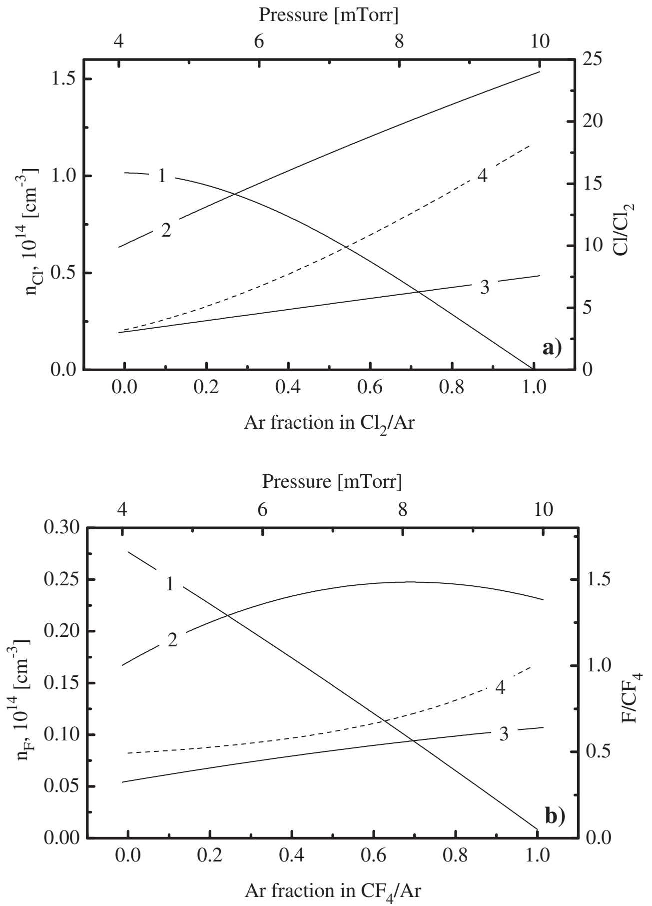

Fig. 6. Model-predicted densities of atomic species in (a) Cl_2/Ar and (b) CF_4/Ar plasmas. Curves 1–3 are the Cl or F atom densities as functions of the (1) Ar mixing ratio or (2, 3) gas pressure, where (2) represents halogen-rich plasmas (20% Ar), and (3) represents Ar-rich plasmas (80% Ar). Curves (4) show the Cl/Cl_2 or F/CF_4 ratios. The other process conditions are the same as in Fig. 1.

a noticeable decrease in ν_{dis}, especially for the CF_4-rich plasmas, because of the deeper drop in n_e (16.3–5.8 s^{-1} for the 20% Ar gas mixture and 49.2–31.9 s^{-1} for the 80% Ar gas mixture at $p = 4$–10 mTorr). Therefore, the F atom density growth is weaker than the n_{Cl} growth and even shows a tendency to saturation in CF_4-rich plasmas. Under the same operating conditions, the Cl atom density in the Cl_2/Ar plasma ($n_{Cl} = 1.0 \times 10^{14}$–$2.9 \times 10^{13}\,cm^{-3}$ for 0–90% Ar) was found to be much higher than the F atom density in CF_4/Ar plasma ($n_F = 2.8 \times 10^{13}$–$7.5 \times 10^{12}\,cm^{-3}$ for 0–90% Ar). As mentioned above, this is because of the differences in k_{dis} and υ_{dis} resulting from the higher threshold energies and lower cross sections of R2 and R7 compared with those of R5 and R6.

Thus, the above data show that there are no non-monotonic changes in the kinetics and densities of charged and neutral species in Cl_2/Ar and CF_4/Ar plasmas within the range of experimental conditions investigated.

3.3 Etching mechanism approaches

To associate the plasma diagnostics data and modeling with the changes in the etching rate, one can use the simple relationships between these parameters given in the literature.[18,20,21] For our case, the basic principles can be formulated as follows:

1) The efficiency of the chemical etching pathways in Cl_2/Ar and CF_4/Ar plasmas can be characterized by the parameter $\gamma_{R,Cl}\Gamma_{Cl}$ or $\gamma_{R,F}\Gamma_F$, respectively. Here, Γ is the flux of atomic species, and γ_R is the reaction probability. For a given type of reaction product, constant surface temperature, and constant fraction of free surface, γ_R is constant. In this case, the rate of the chemical reaction is determined only by the change in Γ_{Cl} or Γ_F. If the etching rate follows Γ_{Cl} or Γ_F, the neutral-flux-limited etching regime of the chemical reaction appears. This situation is typical of an etching process where the external factors (surface temperature and ion bombardment) provide effective cleaning of reaction products from the surface.[18,19]

2) The efficiency of the physical etching pathway is controlled by $Y_s\Gamma_+$, where Y_s is the average sputtering yield,

© 2014 The Japan Society of Applied Physics

and Γ_+ is the total flux of positive ions on the etched surface. For an ion bombardment energy $\varepsilon_i < 500$ eV, one can assume Y_s to be proportional to the momentum transferred by an incident ion to a surface atom.[20,21] Therefore, the relative behavior of the physical etching pathway can be characterized by the parameter $m_i\sqrt{\varepsilon_i}\Gamma_+$ (namely, the ion energy flux), where $\varepsilon_i \approx e|-U_f - U_{dc}|$ is contributed by the applied dc bias $-U_{dc}$ and floating potential $-U_f$. The ion flux Γ_+ can be expressed in terms of the measured n_+ as $\Gamma_+ \approx h_L n_+ v$, where v is the ion Bohm velocity,[13,17] and h_L is the dimensionless correction factor for the ion density at the plasma sheath edge.[13,17] The chemical reaction is said to be in the ion-flux-limited regime when the etching rate follows $m_i\sqrt{\varepsilon_i}\Gamma_+$. This situation is frequently realized for an etching process that forms low-volatility reaction products.

The modeling results show that the behavior of Γ_{Cl} or Γ_F versus both the Ar fraction and the gas pressure generally correspond to the changes in n_{Cl} or n_F shown in Fig. 6. Therefore, the dilution of Cl_2 or CF_4 by Ar results in a monotonic decrease in the efficiency of the chemical etching pathway, whereas an increase in the gas pressure causes the opposite effect. The smaller gap between the fluxes compared with the volume densities of the corresponding species ($\Gamma_{Cl}/\Gamma_F = 2.6$ vs $n_{Cl}/n_F = 3.6$ for pure gases at $p = 6$ mTorr) is associated with higher thermal velocities for F atoms because of their lower mass.

It was also found that though the Cl_2-rich plasmas provide higher n_+ than the CF_4-rich plasmas, the ion fluxes in these systems have an opposite ratio. This is because of the higher ion Bohm velocities (due to higher T_e) and h_L (due to lower plasma electronegativity) in the CF_4-rich plasmas. An increase in the Ar fraction results in a monotonic increase in Γ_+ (1.7×10^{15}–2.3×10^{16} cm^{-2} s^{-1} for Cl_2/Ar and 3.0×10^{15}–2.3×10^{16} cm^{-2} s^{-1} for CF_4/Ar at 0–100% Ar and $p = 6$ mTorr), and an increase in the gas pressure is accompanied by a monotonically decreasing ion flux. In the last case, an increasing or constant n_+, plotted in Fig. 5, is overcompensated for by the decrease in both the ion Bohm velocity (due to the reduced T_e) and h_L (due to the decreasing ion mean free path). As can be seen from Fig. 7, the values of $|-U_{dc}|$ for CF_4-based plasmas are higher than those for Cl_2-based plasmas (for example, 302–148 V for 0–100% Ar in Cl_2/Ar plasma and 360–148 V for 0–100% Ar in CF_4/Ar plasma). Therefore, the CF_4-Ar plasma provides significantly higher values of $m_i\sqrt{\varepsilon_i}\Gamma_+$, and hence higher efficiencies of the physical etching pathway, including the ion-stimulated desorption of reaction products. Note that the changes in the ion energy flux with changes in the Ar fraction and gas pressure are monotonic and similar in both gas systems.

A comparison of Figs. 1, 6, and 7 shows that the non-monotonic Mo etching rates are not directly correlated with either $m_i\sqrt{\varepsilon_i}\Gamma_+$ or the fluxes of atomic species. In our opinion, this indicates the transitional regime of the ion-assisted chemical reaction, where the etching rate is controlled by the neutral and ion fluxes together. In this regime, as reported previously,[18,22] the monotonic but opposite changes in $m_i\sqrt{\varepsilon_i}\Gamma_+$ and Γ_{Cl} or Γ_F can easily lead to non-monotonic etching rates with maxima at various positions on the X axis. The following mechanism of this phenomenon, for example, for the effect of the gas mixing ratio, may be proposed. In Cl_2- or CF_4-rich plasmas, an increase in

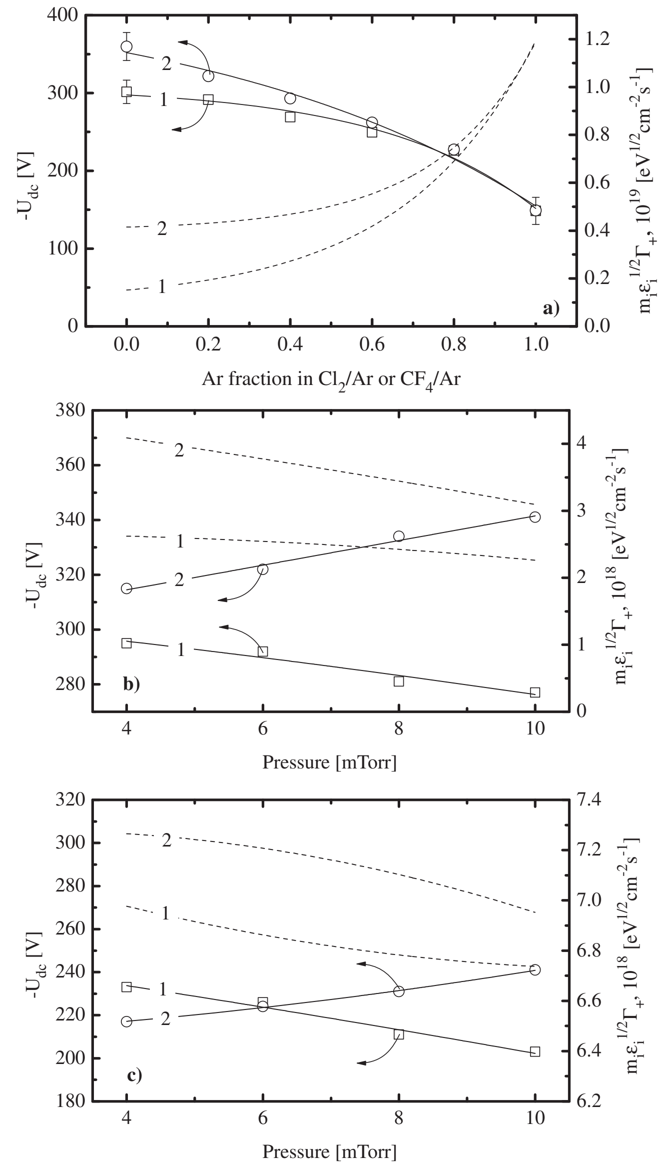

Fig. 7. Measured negative dc bias voltages and model-predicted ion energy fluxes as functions of (a) Ar fraction and (b, c) gas pressure in (1) Cl_2/Ar and (2) CF_4/Ar plasmas. (b) Corresponds to halogen-rich plasmas (20% Ar), and (c) represents Ar-rich plasmas (80% Ar). The other process conditions are the same as in Fig. 1.

$m_i\sqrt{\varepsilon_i}\Gamma_+$ increases the ion-stimulated desorption rate for reaction products and thus increases the fraction of the surface acceptable for chemical reaction with Cl or F atoms. Further, this increases the reaction probability and accelerates the etching despite the decreases in Γ_{Cl} and Γ_F. Because ion-stimulated desorption is the limiting stage of the entire etching process, the CF_4-containing plasma provides a higher etching rate, which follows from the comparison of the $m_i\sqrt{\varepsilon_i}\Gamma_+$ values for our gas systems. With further addition of Ar, the reaction probability reaches saturation at the clear surface, and the Mo etching rate falls because of the lack of Cl or F atoms. In this regime, the Mo etching rate in CF_4/Ar plasma appears to be lower than that for Cl_2/Ar, as predetermined by the difference in the Γ_{Cl} and Γ_F values. Moreover, because the Cl_2/Ar plasma has a higher formation rate for the reaction products (because of the higher Γ_{Cl}) and a lower ion-stimulated desorption rate (because of the

© 2014 The Japan Society of Applied Physics

lower $m_i\sqrt{\varepsilon_i}\Gamma_+$), a more Ar-diluted mixture is needed to obtain a clean surface. Thus, for the Cl_2/Ar plasma, the etching rate maximum is shifted toward higher Ar mixing ratios.

Finally, we emphasize that the analysis above does not provide an exact solution for understanding the Mo etching mechanism because it is based on qualitative correlations. To obtain a quantitative comparison of the etching kinetics in the investigated gas systems, a more comprehensive model of the surface processes (for example, that provided in our previous work[22,23]) should be applied. However, such a model requires data on the sticking coefficients of Cl and F atoms on the Mo surface, which are not accessible yet. Thus, the practical value of this study is that we have estimated the transitional regime of the ion-assisted chemical reaction for both gas chemistries and provided evidence that the non-monotonic etching rates are not associated with the corresponding behavior of the fluxes of plasma active species.

4. Conclusions

In this work, we investigated the etching characteristics and mechanism for Mo thin films in Cl_2/Ar and CF_4/Ar ICPs at $p = 6$ mTorr, $W = 700$ W, and $W_{dc} = 200$ W. The gas mixing ratio was used as the main variable parameter. For both gas mixtures, an increase in the Ar mixing ratio was found to result in a non-monotonic change in the Mo etching rate, with maximum values of 165 nm/min at 60% Ar in Cl_2/Ar and 305 nm/min at 20% Ar in CF_4/Ar. The parameters and compositions of both Cl_2/Ar and CF_4/Ar plasmas were investigated using a combination of plasma diagnostics by LPs and zero-dimensional plasma modeling. Changing the Ar mixing ratio in both Cl_2/Ar and CF_4/Ar plasmas was found to result in qualitatively similar monotonic changes in the efficiencies of both the chemical and physical etching pathways. An analysis of the correlations between the Mo etching rate and the model-predicted fluxes of plasma active species indicates the transitional regime of the ion-assisted chemical reaction, and the non-monotonic changes in the etching rates are probably due to the opposing changes in the reactive neutral flux and ion energy flux.

Acknowledgments

This work was supported by the Industrial Strategic Technology Development Program (10041681, Development of fundamental technology for 10 nm process semiconductor and 10 G size large area process with high plasma density and VHF condition) funded by the Ministry of Knowledge Economy (MKE, Korea).

1) J. W. Lim, S. J. Yun, and J. H. Lee, ETRI J. **27**, 118 (2005).
2) A. Picard and G. Turban, Plasma Chem. Plasma Process. **5**, 333 (1985).
3) E. Gerritsen, N. Emonet, C. Caillat, N. Jourdan, M. Piazza, D. Fraboulet, B. Boeck, A. Berthelot, S. Smith, and P. Mazoyer, Solid-State Electron. **49**, 1767 (2005).
4) Y. H. Kim, C. Y. Sohn, J. W. Lim, S. J. Yun, C.-S. Hwang, C.-H. Chung, Y.-W. Ko, and J. H. Lee, IEEE Electron Device Lett. **25**, 550 (2004).
5) H. P. Loebl, C. Metzmacher, R. F. Milsom, P. Lok, and A. Tuinhout, Electron. Mater.: Sci. Technol. **9**, 115 (2005).
6) A. J. Van Roosmalen, J. A. G. Baggerman, and S. J. H. Brader, *Dry Etching for VLSI* (Plenum Press, New York, 1991).
7) D. S. Fischl and D. W. Hess, J. Vac. Sci. Technol. B **6**, 1577 (1988).
8) S.-J. Park, C. P. Sun, J. T. Yeh, J. K. Cataldo, and N. Metropoulos, MRS Proc. **68**, (1986).
9) M. Sugavara, *Plasma Etching: Fundamentals and Applications* (Oxford University Press, New York, 1998).
10) M. Kim, N. K. Min, S. J. Yun, H. W. Lee, A. Efremov, and K.-H. Kwon, Microelectron. Eng. **85**, 348 (2008).
11) A. Efremov, N.-K. Min, B.-G. Choi, K.-H. Baek, and K.-H. Kwon, J. Electrochem. Soc. **155**, D777 (2008).
12) E. O. Johnson and L. Malter, Phys. Rev. **80**, 58 (1950).
13) C. Lee and M. A. Lieberman, J. Vac. Sci. Technol. A **13**, 368 (1995).
14) M. A. Lieberman and S. Ashida, Plasma Sources Sci. Technol. **5**, 145 (1996).
15) A. M. Efremov, G.-H. Kim, J.-G. Kim, A. V. Bogomolov, and C.-I. Kim, Microelectron. Eng. **84**, 136 (2007).
16) A. M. Efremov, D.-P. Kim, and C.-I. Kim, Vacuum **75**, 133 (2004).
17) M. A. Lieberman and A. J. Lichtenberg, *Principles of Plasma Discharges and Materials Processing* (Wiley, New York, 1994).
18) A. Efremov, D. P. Kim, and C.-I. Kim, IEEE Trans. Plasma Sci. **32**, 1344 (2004).
19) T. Sugano, *Applications of Plasma Processes to VLSI Technology* (Wiley, New York, 1990).
20) C. Lee, D. B. Graves, and M. A. Lieberman, Plasma Chem. Plasma Process. **16**, 99 (1996).
21) W. Jin, S. A. Vitale, and H. H. Sawin, J. Vac. Sci. Technol. A **20**, 2106 (2002).
22) S. Kang, A. Efremov, S. J. Yun, J. Son, and K.-H. Kwon, Plasma Chem. Plasma Process. **33**, 527 (2013).
23) A. M. Efremov, D.-P. Kim, and C.-I. Kim, Thin Solid Films **474**, 267 (2005).

© 2014 The Japan Society of Applied Physics